ICIC Express Letters
Volume **13**, Number **7**, July **2019**

ICIC International ©2019 ISSN 1881-803X
pp. **539–546**

POWER TRANSFER MAXIMIZATION OF THERMOELECTRIC GENERATOR SYSTEM USING PEAK TRAPPING AND SCANNING-BASED MPPT ALGORITHMS

Faizal Arya Samman[1,*], Wahyu Haryadi Piarah[2] and Zuryati Djafar[2]

[1]Department of Electrical Engineering
[2]Department of Mechanical Engineering
Universitas Hasanuddin
Jl. Poros Malino Km. 6, Bontomarannu 92171, Gowa, Indonesia
[*]Corresponding author: faizalas@unhas.ac.id

Received November 2018; accepted January 2019

Abstract. *Power transfer maximization method of a heat recovery system based on thermoelectric generator (TEG) patches using peak trapping or peak bracketing and scanning-based maximum power point tracing (MPPT) algorithms is presented in this paper. The MPPT algorithms operate based on perturb-and-observe (P&O) methodology. An electronic control unit (ECU), in which the MPPT algorithm will be embedded, perturbs an electronic switch (a transistor) in a switched-mode DC-DC converter with pulse signals with variable duty ratio. The MPPT unit will control the pulse duty-ratio based on the observations of the converter output power until finding a certain duty-ratio, which drives the system such that it operates its peak or maximum power point (MPP). By decrementing the duty-ratio step-size and changing the step-number for each scanning-step iteration, the proposed MPPT algorithm can trap the maximum power points. Five types of the MPPT algorithms are proposed, designed and verified through simulations. Appropriate selections of the variable step size can potentially improve the convergence speed of the algorithms. The peak-bracketing (peak trapping) MPPT algorithm, can reach the MPP after 19 P&O-steps and outperforms the other types of the proposed scanning-based MPPT algorithms. The implementation of the algorithms will not require multiplication and division operations, resulting in a very low computing energy and complexity.*
Keywords: Heat recovery, Thermoelectric generator, Maximum power point tracing, Embedded electronic control unit

1. **Introduction.** Renewable energy has been an interesting issue recently. The reduction of fossil fuel resources and the environment issue are the main reasons of the emerging issue. Renewable energies resources can be found, e.g., from solar, wind, tide, geotherm, hydro as well as micro-hydro. Solar radiation seems to be the main energy resources for earth. It derives secondary energies such as wind and tide, which emerge because of different earth pressure or temperature, resulted from different sun radiations on the earth. Other example is bioethanol, which is originally produced from photosynthesis process, which naturally uses sun radiation.

Besides the aforementioned energy sources, exhausted heat or thermal energy meanwhile exists every where around our environments and industries. We can find some exhausted heat energies, e.g., from combustion engine bodies in automotive and industries, exhaust gas pipes in vehicles, and also from other exhausted heat sources produced from combustion processes. Exhausted heat due to the sun radiation can also be found, e.g., from alloy-made house rooftops, car body, and windows glasses of buildings. From supercomputer stations, we can also find it significantly. The exhausted thermal energy can

DOI: 10.24507/icicel.13.07.539

be recovered (harvested) to be useful electric energy by using, for instance, thermoelectric generator (TEG) patches.

Thermal energy harvesting from the TEG patches using maximum power point tracing (MPPT) algorithms embedded on an electronic control unit is presented in this paper. A thermo-mechanical model of a TEG is shown in Figure 1(a). The semiconductor materials between the heat and cold sides of the TEG patch will be triggered to generate electric power, due to temperature difference between both sides. A TEG patch owns specific power characteristic. Its maximum power operation point is located on a certain voltage-current point. Hence, operating a TEG patch at that point is necessary.

A new idea to operate the TEGs at its maximum power point by using effective and low complex maximum power point tracing (MPPT) algorithms is presented in this paper. Some sections are then arranged to expose the idea as follows. Section 2 exposes research works related to the MPPT techniques for TEGs. Section 3 explains the TEG's power characteristics, the thermal mechanical model and its equivalent electric circuit model. The proposed MPPT algorithms, namely peak trapping or peak bracketing and decremented window-size scanning-based MPPT algorithm are exposed in Section 4. Section 5 presents the simulation results. Section 6 finally concludes the work and gives a brief outlook.

2. **Related Works and Contribution.** A digital or an analog electronic control unit (ECU) can be used to implement an MPPT algorithm for thermoelectric generator (TEG) systems [1]. The analog MPPT control unit is simple and has low design cost. However, it has a few drawbacks. Analog circuit is sensitive to the parameter drifts (due to aging) and external noise signals. We propose MPPT algorithms that can be implemented in programmable electronic control unit such as microcontroller and programmable logic devices. Compared to the analog counterpart, digital techniques are less sensitive to the parameter drifts and noises.

So far, there are some techniques used to control TEG operation at its peak or maximum power point. They are for instances incremental conductance [2], fractional open-circuit voltage [3, 4], fractional short-circuit current [5], extremum seeking control mechanism [6], a simple MPPT method [7] that operates a control circuit on a pre-programmed locus near the maximum power point (MPP) and P&O methods or combined P&O-OCV [8] that uses the fast tracking capability of the OCV method. The fractional open-circuit voltage (OCV), fractional short-circuit current (SCC) and pre-programmed locus technique are simple, but the flexibility of the above techniques is low. The OCV and SCC must be recognized before implementation. Hence, for different TEG operating states and TEG configurations, the OCV and SCC must be measured in advanced.

The MPPT method presented in [9] does not use an MPPT algorithm to maintain TEG operation at its maximum voltage-power point. The charge pump is only used to regulate the circuit output voltage. Therefore, the method will not be suitable for a TEG system with dynamic maximum power point conditions and variable structures of TEG's array.

MPPT methods that operate based on P&O techniques and are independent from the operating conditions and the changes of TEG arrangement. Our proposed MPPT methods are named as peak trapping or peak bracketing and decremented window-size scanning-based (DWS) MPPT algorithms. The peak trapping and the DWS-based MPPT algorithm are simple and flexible to implement. Compared to the fractional OCV and SCC, the implementation is more flexible. It does not need prior information about the TEG's arrangement and load conditions.

The work in [10] and [11] uses adaptive mechanism to scale the duty ratio of the converter's PWM signal. Our proposed techniques require only regular iterative algorithms, which are simple to implement. The existence of the adaptive mechanism will surely improve the MPPT performance, but their computational complexity becomes larger.

The previous version of our proposed MPPT algorithm has been successfully applied in our another research work using photovoltaic system. The current version is also applied successfully in a TEG system, which is presented in this paper, with new contribution to the convergence speed improvement. A new approach by varying the duty-ratio step-number and step-size decrements is proposed and used to improve the tracking speed of the algorithms to reach the expected global maximum power points.

3. **TEG Modelling and Power Characteristics.** This section presents a few stages to model a single TEG panel/patch and an array structure of TEG patches. An equivalent electric circuit diagram is firstly modeled. This model is used to obtain the power characteristics of the TEG patch. In line with a DC/DC converter circuit, an array of TEG patches is arranged and simulated by using SPICE (Simulation Program with Integrated Circuit Emphasis) software. For advanced research objective, the TEG model can also be utilized to improve the TEG structure that can give an optimized TEG's power characteristic [13]. The following subsections discuss the simulation results.

3.1. **Single TEG patch model.** The thermo-mechanical diagram of a TEG patch is presented in Figure 1(a). Its equivalent electric circuit is presented in Figure 1(b). The TEG patch is modeled in a single circuit loop with a temperature-dependent voltage source (V_{EQ}) connected in series with a temperature-dependent resistor (R_{EQ}). The V_{EQ} and R_{EQ} variables are dependent on the temperature difference (ΔT) between the TEG's hot and cold side as presented in Equation (1) and Equation (2), respectively [14].

$$V_{EQ} = \alpha \Delta T \frac{\theta_m}{\theta_m + 2\theta_c} \tag{1}$$

$$R_{EQ} = R_E + \alpha^2 \theta_m \theta_c \frac{T_H + T_C}{\theta_m + 2\theta_c} \tag{2}$$

The parameters of the equations are explained as follows:

α: Seebeck coefficient, depends on the P-N semiconductor material

θ_m: internal thermal resistance

θ_c: contact thermal resistance, which is the contact used to connect the TEG panel to the thermal energy source

R_E: electric resistance, consists of P-N semiconductor resistance and contact resistance, which is the contact used to connect the TEG panel and the load

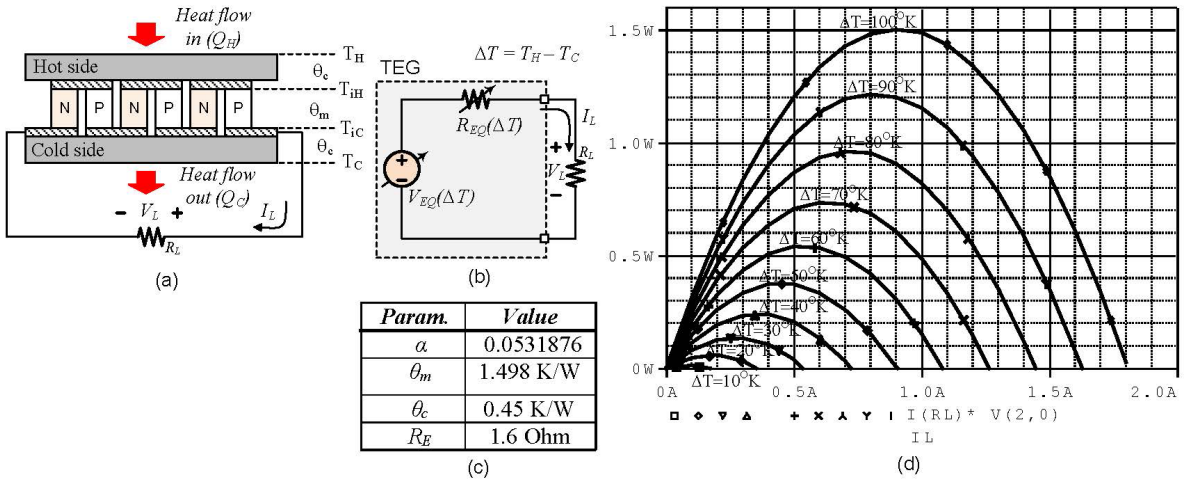

Param.	*Value*
α	0.0531876
θ_m	1.498 K/W
θ_c	0.45 K/W
R_E	1.6 Ohm

(c)

FIGURE 1. (a) The single TEG patch thermal mechanical model, (b) its equivalent electric circuit model, (c) the parameter values used in the simulation, and (d) its power curve characteristic

The temperature difference between the TEG's hot and cold side is formulated as follows.

$$\Delta T = T_H - T_C \tag{3}$$

By substituting Equation (3) into Equation (2), then we obtain Equation (4).

$$R_{EQ} = R_E + \alpha^2 \theta_m \theta_c \frac{\Delta T + 2T_C}{\theta_m + 2\theta_c} \tag{4}$$

Equation (1) and Equation (4) are modeled and simulated in SPICE. The TEG parameters for simulation are presented in a table shown in Figure 1(c). Figure 1(d) shows the power curve profile of the TEG after the simulation. As shown in the figure, larger temperature difference will give larger output power. A peak or maximum power point appears also at each power curve. It seems that for every temperature case, there is a peak power point that can be achieved when the TEG is operated at certain current point. This point is named as maximum power point (MPP) and is the expected point of the TEG operation. The phenomenon is the background of using a maximum power point tracing (MPPT) algorithm used to control the TEG operation at the expected maximum power point. Section 4 will discuss later the topic.

3.2. **TEG array model.** This section presents the power curve characteristic of a TEG array. The TEGs are arranged in a 2×4 array structure. Two branches are connected in parallel, where at each branch, there are four TEG patches in series. The power curve characteristic is presented in Figure 2. Larger temperature differences (ΔT) provide higher maximum output powers, which is similar to the simulation result before. At each power curve, there is a peak (maximum) output power, which occurs at certain current point.

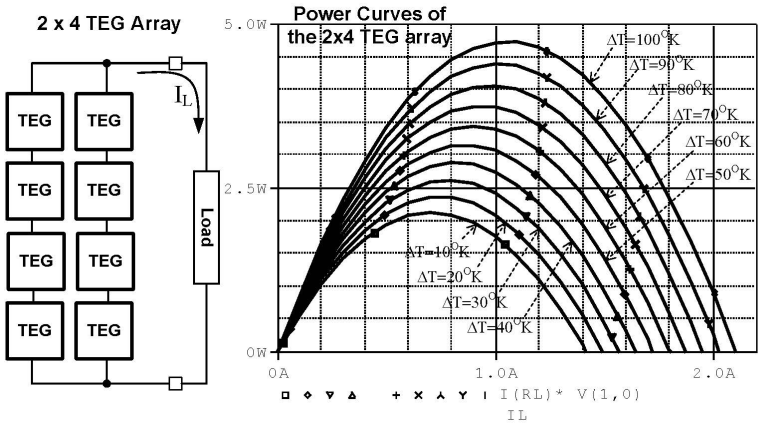

FIGURE 2. Power curves of the TEG patch array (2×4) for variable temperature differences

3.3. **TEG array power profile with a DC-DC converter circuit.** This section will discuss a technique to control the TEG operation at its MPP. The MPP occurs at certain voltage or current point. Therefore, a switched-mode DC/DC converter is required to control the TEG current or voltage at the MPP. Theoretically, the DC/DC converter is utilized to drive the internal impedance (input impedance) of the TEG such that it will match with load impedance. The impedance matching procedure is undertaken by applying a pulse width modulated (PWM) signal to the MOSFET's gate terminal in the converter circuit. When the impedance matching occurs, the maximum power transfer will take place.

Some types of DC/DC converters can be used in system. In our case, we use a single-ended primary inductive converter (SEPIC). The circuit topology of the SEPIC is presented in Figure 3. The SEPIC input port is connected to the TEG and its output port

is connected to the load (R_L). As shown in the figure, the PWM signal that has period of t_P with t_{ON} duty ratio is supplied to the gate terminal of MOSFET M_1. The duty cycle ratio of the PWM signal is $\frac{t_{ON}}{t_P} \times 100\%$.

When the load R_L is set 50Ω and 100Ω, and the ΔT is set 100°K, the SEPIC, the load and the TEG are simulated by changing the duty ratio of the PWM signal from 10% until 90%. The diagrams on the right-hand side in Figure 3 show the power curve characteristics of the SEPIC and TEG output terminals. It seems that there is a duty cycle ratio point, in which the TEG and SEPIC transfer a maximum output power to the load R_L. It seems also that the maximum (duty-ratio/power) point is different for different load values.

As shown in the power curve diagram on the right-hand side of Figure 3, the maximum power point for the case of $R_L = 50\Omega$ is about 8.05W at 76% PWM duty ratio, and for the case of $R_L = 100\Omega$ is about 8.05W at 80% PWM duty ratio. The main objective of the design is to drive the duty ratio of the PWM signal such that it will automatically end up at the expected duty ratio and peak power point. Hence, a control algorithm which is embedded on the electronic control unit (ECU) is required to fulfill the objective. Figure 4 illustrates the SEPIC circuit accompanied with the electronic control unit (ECU).

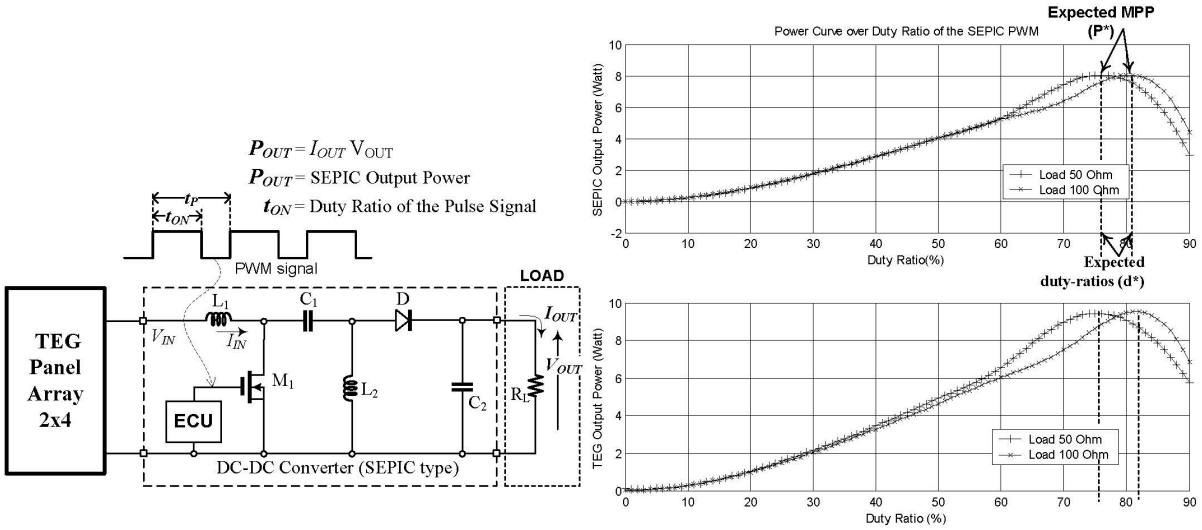

FIGURE 3. The TEG-SEPIC circuit schematic (left-hand side), and its power curve characteristic with different duty ratio (right-hand side)

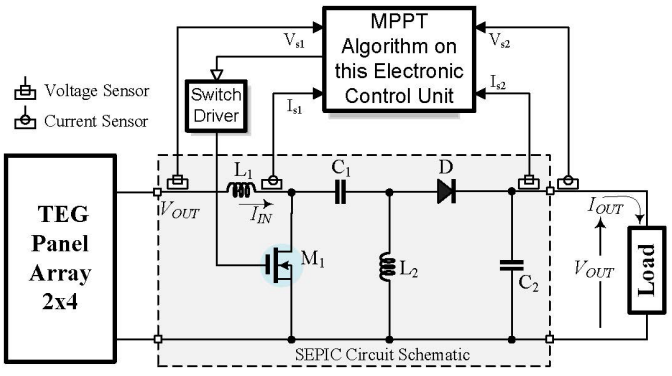

FIGURE 4. The schematic of the MPPT unit with SEPIC and TEG patches

4. **The Peak Trapping and Scanning-Based MPPT Algorithms.** As shown in Figure 4, the MPPT algorithm is embedded on the ECU. The output or load voltage (V_{OUT}) and load current (I_{OUT}) are sensed respectively using voltage and current sensors. The power value (P_{OUT}) is obtained by multiplying the measured voltage and current. The ECU will perturb the SEPIC with a PWM signal having a certain duty ratio. Afterwards, the ECU observes the load voltage and current of the SEPIC, and then calculates the output power. In every perturb repetition, the ECU will obtain the power value and compare it with the previous measurement. The ECU saves the tentative power point and duty ratio point in each P&O step. By using the iterative steps, the expected MPP will be finally reached.

The implementation of the DWS-based MPPT algorithm is simple and can be easily derived into several step modes. The domain or window of P&O scanning of the algorithm is decremented for each iteration scan. Therefore, the step-size and the step number of the P&O scanning mechanism change dynamically in every scan step. Due to the step size decrements, the proposed algorithm is called decremented window-size scanning (DWS).

We proposed five techniques to implement the MPPT algorithms. Four of them are DWS methods. Each of them has different number of scanning iteration and different size of decremented windows scanning. Another MPPT algorithm called peak trapping or peak bracketing with initial scanning (PBIS) is also introduced for comparative study. The PBIS scans initially the power points to find 3 highest bracketing points that will be used in the next step to trap the MPP. The trapping mechanism is made by half-reducing step-by-step the domain of the highest bracketing points. The differences of the peak trapping and DWS algorithm are summarized in Table 1.

Table 1. The differences of the proposed PBIS and DWS-based MPPT algorithms

Method	Step-size sequential decrement	Step-number sequential change	Number of scan-step iterations
DWS method 1	20-10-5-2-1	5-5-5-5-5	5
DWS method 2	10-4-2-1	9-6-5-5	4
DWS method 3	10-1	9-19	2
DWS method 4	13-4-1	7-7-7	3
PBIS method	16-8-4-2-1	6-3-3-3-3	5

The step-size decrement is the order of the step-size decremented for the next P&O scan-step iteration. The DWS method 2 for example has the step-size decrement values of 10-4-2-1 (4 ordered decrement values). For every P&O scan-step iteration, the step-size values are variably decremented from 10, 4, 2 and 1 duty ratio step-size. The minimum density of the duty ratio step-size is set to 1%. The step number is the number of P&O step undertaken for each scan-step iteration. The number of scan-step iteration (as shown in Table 1) is in accordance with the number of ordered step-size decremented values.

5. **Simulation Results.** This section discusses the simulation testing of our proposed PBIS and DWS algorithms that track the MPPs of the power curves presented previously on the right-hand side of Figure 3, i.e., the power curves for the TEG system with 50Ω and 100Ω load resistances.

Figure 5(a) presents the simulation result for 50Ω resistance load value. As shown in the figure, the DWS algorithms 1, 2, 3 and 4 can reach the same MPP, i.e., about 8.0524 Watt at 76% PWM's duty ratio point, although they give different power and duty ratio tracking lines. Table 2 summarizes the performances of the peak trapping (PBIS) and DWS-based MMPT algorithms.

Figure 5(b) shows the simulation result for 100Ω resistance load value. As presented in the figure, the DWS algorithms 1, 2, 3 and 4 can again reach the same MPP, i.e., about

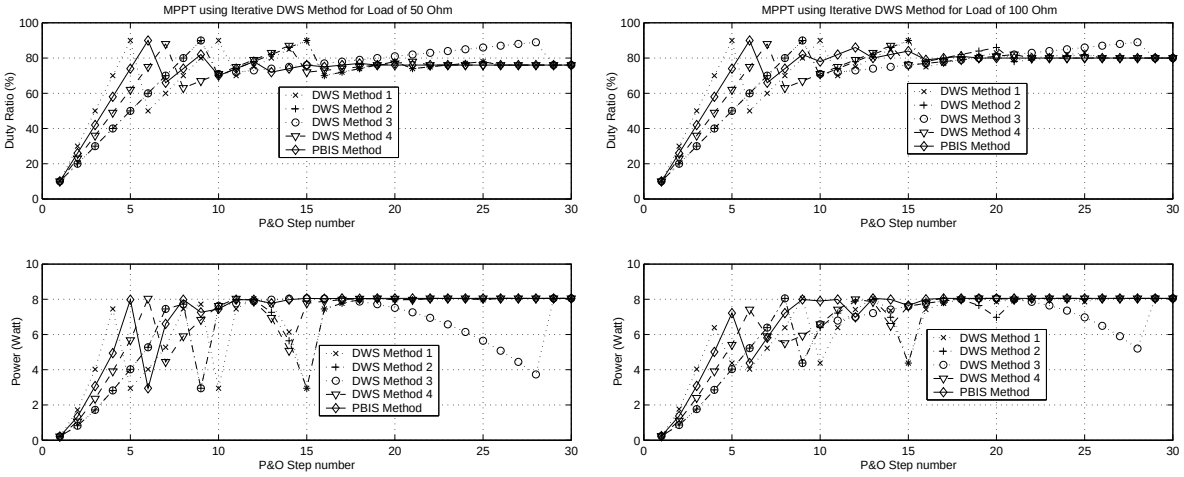

(a) Simulation with load 50Ω (b) Simulation with load 100Ω

FIGURE 5. The simulation results for 50Ω and 100Ω resistance loads

TABLE 2. The performance comparison of the DWS-based MPPT algorithms

Method	Reached power	Final duty ratio	Number of P&O-steps
DWS method 1	8.0524W	76%	26
DWS method 2	8.0524W	76%	26
DWS method 3	8.0524W	76%	29
DWS method 4	8.0524W	76%	22
PBIS method	8.0524W	76%	19

8.0538 Watt at 80% PWM's duty ratio, with different power and duty ratio tracking lines. As shown in the figure, the PBIS and DWS method 1, 2 and 4 can track the MPP faster than the DWS method 3.

It seems that from both simulation, all of the MPPT algorithms can automatically tune the duty cycle ratio of the PWM signal at an expected maximum power point. The performance comparison between the PBIS and the DWS-based MPPT algorithms for 50Ω load resistance value is shown in Table 2. The obtained output power (the expected MPP) at the final duty ratio of the PWM signal, as well as the number of P&O-steps to attain the MPP are presented in the table. The PBIS method gives better performance than the other DWS methods in term of the convergence speed. The PBIS method needs the least number of P&O-steps (19 steps), to reach the MPP. All MPPT methods can reach however the same 8.0524W output power at 76% PWM duty ratio.

For 100Ω load resistance, the same performance is achieved. The PBIS and DWS methods 1, 2, 3 and 4 need respectively 19, 26, 26, 29 and 22 P&O-steps to reach the MPP. However, the PBIS and DWS methods can attain the same 8.0538W peak power point, at the same 80% duty ratio.

6. **Conclusions.** Under different load conditions, the proposed DWS-based and peak trapping/bracketing MPPT algorithms can tune automatically the duty-ratio of the PWM signals to approach the expected MPP. By using our proposed MPPT methods, the expected MPP will be finally bracketed or trapped in the a domain scan, which is gradually reduced step-by-step. The trapping process is achieved with relatively small number of P&O-steps. Our proposed DWS-based MPPT methods can attain the MPP at about 22 until 29 P&O-steps. While the peak bracketing or peak trapping method with initial

large-step scanning can reach the MPP at about 19 P&O-steps, lower than the DWS-based methods.

The simulation is made using 1% minimum duty-ratio step-size. A lower minimum duty ratio step-size can be further chosen. The lower duty ratio step-size values could probably only result in slightly small differences of the MPP accuracy. When the minimum duty-ratio step-size is set constant, then for each different loading condition and TEG configuration, the number of P&O-steps to reach the MPP is almost equal.

Acknowledgment. We gratefully acknowledge Universitas Hasanuddin at Makassar for funding this research work under the scheme of the Excellent Research Grant for Patent Publication (*Penelitian Unggulan Berpotensi Paten*) in the year 2017.

REFERENCES

[1] S. Kim, S. Cho, N. Kim and J. Park, A maximum power point tracking circuit of thermoelectric generators without digital controller, *IEICE Electronics Express*, vol.7, no.20, pp.1539-1545, 2010.

[2] S. Twaha, J. Zhu, Y. Yan, B. Li and K. Huang, Performance analysis of thermoelectric generator using DC-DC converter with incremental conductance based maximum power point tracking, *Energy for Sustainable Development*, vol.37, pp.86-98, 2017.

[3] A. Montecucco and A. R. Knox, Maximum power point tracking converter based on the open-circuit voltage method for thermoelectric generators, *IEEE Trans. Power Electronics*, vol.30, no.2, pp.828-839, 2015.

[4] K. Suzuki and M. Deng, Operator-based MPPT control system for thermoelectric generation by measuring the open-circuit voltage, *Proc. of the 2016 International Conference on Advanced Mechatronic Systems (ICAMechS)*, pp.236-241, 2016.

[5] I. Laird and D. D. Lu, High step-up DC/DC topology and MPPT algorithm for use with a thermoelectric generator, *IEEE Trans. Power Electronics*, vol.28, no.7, pp.3147-3157, 2013.

[6] S. Patel, O. Maganga, A. Fofana and I. Bates, Hardware implementation of a constraints-based ESC for thermoelectric generators, *IFAC-PapersOnLine*, vol.50, no.1, pp.6534-6539, 2017.

[7] A. Paraskevas and E. Koutroulis, A simple maximum power point tracker for thermoelectric generators, *Energy Conversion and Management*, vol.108, pp.355-365, 2016.

[8] Y.-H. Liu, Y.-H. Chiu, J.-W. Huang and S.-C. Wang, A novel maximum power point tracker for thermoelectric generation system, *Applied Energy*, vol.97, pp.306-318, 2016.

[9] W. Wang, V. Cionca, N. Wang, M. Hayes, B. O'Flynn and C. O'Mathuna, Thermoelectric energy harvesting for building energy management wireless sensor networks, *Int'l Journal of Distributed Sensor Networks*, vol.2013, pp.1-14, Article ID 232 438, 2013.

[10] T. H. Kwan and X. Wu, The Lock-On Mechanism MPPT algorithm as applied to the hybrid photovoltaic cell and thermoelectric generator system, *Applied Energy*, vol.204, pp.873-886, 2017.

[11] J. H. Carstens and C. Ghmann, Maximum power point controller for thermoelectric generators to support a vehicle power supply, *materialstoday: Proceedings*, vol.2, no.2, pp.790-803, 2015.

[12] F. A. Samman, A. A. Rahmansyah and Syafaruddin, Peak bracketing and decremented window-size scanning-based MPPT algorithms for photovoltaic systems, *International Journal of Innovative Computing, Information and Control*, vol.14, no.3, pp.1015-1028, 2018.

[13] H. Chen, N. Wang and H. He, Equivalent circuit analysis of photovoltaic-thermoelectric hybrid device with different TE module structure, *Advances in Condensed Matter Physics*, vol.2014, pp.1-6, Article ID 824 038, 2014.

[14] S. Siouane, S. Jovanovi and P. Poure, Equivalent electrical circuits of thermoelectric generators under different operating conditions, *Energies*, vol.10, pp.1-15, 2017.